A new high-performance sideband-separating mixer for 650 GHz

R. Hesper[a], A. Khudchenko[a], A.M. Baryshev[a,b], J. Barkhof[a], and F.P. Mena[c]

[a]Kapteyn Astronomical Institute, University of Groningen, The Netherlands
[b]SRON Netherlands Institute for Space Reasearch, Groningen, The Netherlands
[c]Universidad de Chile, Santiago, Chile

ABSTRACT

In the modular sideband-separating mixers that we built over the last years, we observe a clear anti-correlation between the image rejection ratio obtained with a certain block and its noise performance, as well as strong correlations between the image rejection and imbalances in the pumping of the mixer devices.

We report on the mechanisms responsible for these effects, and conclude that the reduction of the image rejection is largely explained by the presence of standing waves. We demonstrate the rejection ratio to be very sensitive to those. In principle, all potential round-trip paths should be terminated in matched loads, so no standing waves can develop. In practice, the typical high reflections from the SIS mixers combined with imperfect loads and non-negligible input/output reflections of the other components give many opportunities for standing waves. Since most of the loss of image rejection can be attributed to standing waves, the anti-correlation with the noise temperature can be understood by considering any excess loss in the structure, as the waveguides start acting as distribured loads. This reduces the standing waves, and thereby improves the rejection ratio, at the expense of noise temperature.

Based on these experiences, we designed a new waveguide structure, with a basic waveguide size of $400\times200\,\mu$m and improved loads. Strong emphasis was placed on low input and output reflections of the waveguide components, in some places at the cost of phase or amplitude imbalance. For the latter there is ample margin not to impair the performance, however. Apart from further details of the design, we present the first results of the new mixers, tested in a modified production-level ALMA Band 9 receiver, and show that even in an unfinished state, it simultaneously meets requirements for image rejection and noise temperature.

Keywords: sideband-separating mixers, waveguide hybrids, submillimeter receivers, ALMA instrumentation

1. INTRODUCTION

In the past we successfully demonstrated a sideband-separating mixer for the frequency range of 600–720 GHz (ALMA Band 9).[1,2] The waveguide structure was based on a classical quadrature hybrid architecture,[3] micromachined into a modular waveguide split-block.[4] It fulfilled the ALMA specifications with respect to noise temperature and image rejection. However, based on the performance of the individual mixer devices, the noise temperature was slightly disappointing, especially in the light of the levels obtained by the ALMA Band 9 DSB production receivers.[5] Apart from the excess noise temperature, a marked anti-correlation was observed of the noise temperature and image rejection ratio (IRR) between mixer blocks of different materials and surface finish.[2]

1.1 Waveguide Losses

For the observed excess loss, two main contributions were identified: material properties and waveguide geometry. On the side of material properties, the gold plating that is customarily applied to waveguide blocks appeared to be detrimental to the waveguide transmission. In contrast, we found the noise performance of unplated copper blocks (even when alloyed with a few percent of tellurium for machinability) to be much better.[2] The second important loss mechanism turned out to be the geometry of the waveguides. These were rather small ($310\times145\,\mu$m), which put the lower edge of the band (600 GHz) close to the waveguide cutoff (484 GHz). While

Correspondence to R.H., email: r.hesper@astro.rug.nl

Millimeter, Submillimeter, and Far-Infrared Detectors and Instrumentation for Astronomy VIII,
edited by Wayne S. Holland, Jonas Zmuidzinas, Proc. of SPIE Vol. 9914, 99140G
© 2016 SPIE · CCC code: 0277-786X/16/$18 · doi: 10.1117/12.2233065

Downloaded From: http://proceedings.spiedigitallibrary.org/ on 10/11/2016 Terms of Use: http://spiedigitallibrary.org/ss/termsofuse.aspx

functionally excellent, what was not taken into account at the time was the behaviour of the losses as function of waveguide size. In the original monolithic design, the waveguide loss was quite tolerable because of the very short stretches of waveguide (order of 6 mm). In the modular design, however, we had to sacrifice some of this compactness in order to create enough space for interfaces and mounting hardware. This increased the total length of the signal path from the horn to the mixers to about 12 mm, thereby doubling the losses.

Some basic simulations (not shown here) demonstrate that the losses indeed go up sharply when approaching the cutoff frequency. It should be noted, however, that modelling waveguide losses at these high frequencies it non-trivial. Even the standard formalisms based on a simple skin-effect model may not be valid anymore, for instance when the calculated skin depth becomes comparable to the electron mean free path in the metal (the so-called "anomalous skin-effect regime"[6,7]). Also surface roughness and stresses or dislocations in the wall material due to machining are likely to play an increasing role at higher frequencies.

Nevertheless, it is obvious that, after choosing a low-loss material, the most important prerequisite for low-loss waveguides at high frequencies is a large size. As a side note, it should be mentioned that another significant factor is the waveguide height. A 4:1 reduced-height waveguide (as, for instance, used in the ALMA Band 9 DSB mixers) can produce similar high losses, compared to a 2:1 full-height one. Of course, in the Band 9 DSB case, the waveguide runs were so short that this did not seriously impact the noise performance.

1.2 Influence of Standing Waves

Another effect that was quite noticeable in our previous mixer assemblies is an anti-correlation between the image rejection ratio and the noise temperature. In gold-plated hybrid blocks, the IRR could approach 20 dB over most of the band, while a bare copper or copper-tellurium block would barely attain 12–15 dB.[2] The noise temperatures of the non-plated blocks were notably better, though.[1]

We attribute the anti-correlation of the noise temperature and the image rejection to the presence of standing waves. The driving observation to this statement is that the strong periodicity that we typically have in the rejection ratio (Ref. [2], figure 5 for instance) seems always correlated with a periodicity in the pumping balance of the two SIS devices. This is especially noticeable when we pump the mixers through the RF input port (rather than the LO port), making us suspect that the main culprit is in the path between the mixers and, most likely, the RF load that terminates the unused port of the hybrid. This is after all the place where the combined coherent reflections from the mixers end up (after passing back and forth through the 90° hybrid). One of the

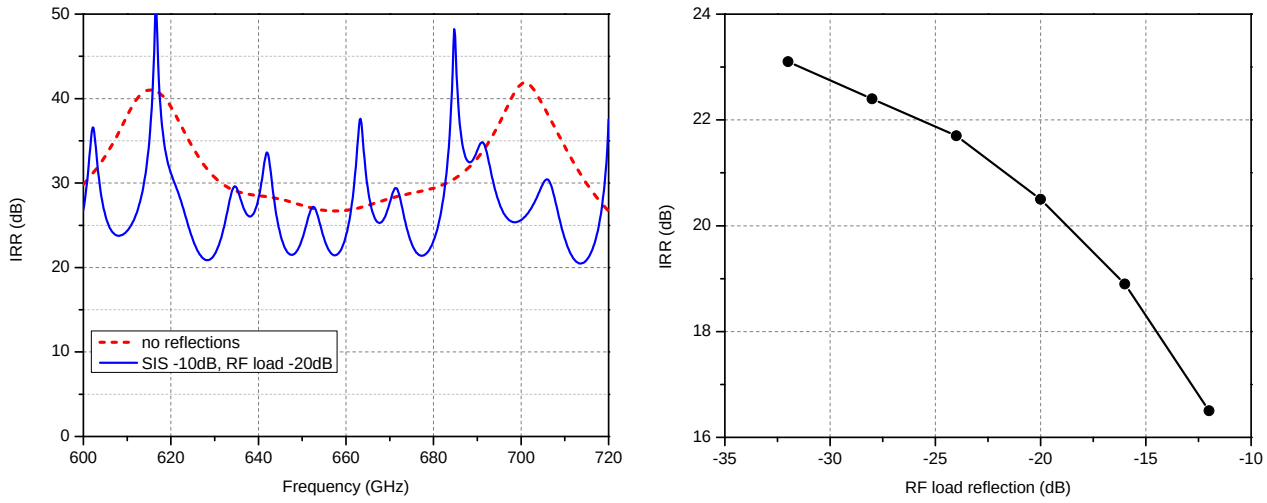

Figure 1. a (left): Simulated contribution to the image rejection ratio of the waveguide structure (*i.e.*, with ideal mixers and IF hybrid). Dotted line: no reflections from both mixers and waveguide loads. Solid line: mixer reflection -10 dB, load reflection -20 dB. Only the RF load is varied, the LO dumps are considered ideal. b (right)The minima of the IRR as determined from curves as in Fig. 1a, as function of the reflection coeficient of the RF load.

Downloaded From: http://proceedings.spiedigitallibrary.org/ on 10/11/2016 Terms of Use: http://spiedigitallibrary.org/ss/termsofuse.aspx

characteristic periods of the pumping balance variations is also quite consistent with the lengths of the waveguide runs involved, while another one correponds closely to the distance between the mixer and the hybrid. Because of these strong correlations, we hypothesize that the highest attainable value of the image rejection in the end is dominated by standing waves.

To verify our suspicions about the detrimental effects of standing waves, we performed a series of model calculations on a slightly simplified structure (of the original design as in Ref. [3]), but with the correct overall dimensions. In this model, both the SIS mixers and the waveguide loads were replaced by tuned mismatches in order to introduce controlled reflections from these components. As an example, figure 1a shows the contribution of the waveguide structure to the image rejection ratio, both for the ideal case (no reflections), and for the case where the SIS mixers are -10 dB reflective and the loads -20 dB, which are realistic estimates. A very marked degradation in the IRR, from close to 30 dB to barely 20 dB can be seen.

We repeated this simulation for varying values of the load reflection coefficient. Figure 1b shows the resulting "worst case" IRRs, *i.e.*, the lowest point of the IRR curve within the band, as function of reflection coefficient. Note that in these calculations the influence of the phase and amplitude imbalances introduced by the mixers and the IF hybrid are not taken into account, and the calculated IRR should be seen as a figure of merit.

Since we can attribute most of the loss of rejection ratio to the presence of standing waves, based on these simulations, the anti-correlation with the noise temperature becomes obvious: when there is excess loss in the structure, the waveguides start acting like a distributed load, reducing the standing waves, and thereby improving the rejection ratio. At the same time, however, the noise temperature suffers.

2. DESIGN CONSIDERATIONS

2.1 Standing Wave Paths

The following major standing wave paths can be identified (for the locations of the parts in the structure, see Fig. 2):

1. Mixers — through hybrid — RF load
2. Mixer — hybrid
3. Mixer — LO coupler
4. Mixer — through LO coupler — LO splitter
5. LO splitter — LO coupler
6. LO splitter — LO load

These are the paths which have at least one moderately reflective end, namely either one of the mixers or one of the output ports of the LO splitter. Since both are not easy to improve, it is clear that any contribution to the reduction of the standing waves should come from the other side of the loop.

Standing waves in paths 2, 3 and 5 can be minimized by optimizing the input reflections of the hybrid and the LO coupler, which therefore is made into one of the major design drivers. Since the LO splitter is inherently reflective, path 4 can only be reduced by decreasing the coupling coefficient of the LO coupler. As discussed below, this can nowadays be done because of the increased power of currently available LO sources. The two remaining paths, 1 and 6, depend on the reflection of the loads. It should be noted that in path 1, because of symmetry, the reflections of both mixers combine in phase into the RF load. This means that all energy reflecting off the mixers ends up here, while none of it exits the RF feedhorn. Because even relatively weak standing waves can modify phase and amplitude of the input signal considerably, this path is clearly of major concern.

Downloaded From: http://proceedings.spiedigitallibrary.org/ on 10/11/2016 Terms of Use: http://spiedigitallibrary.org/ss/termsofuse.aspx

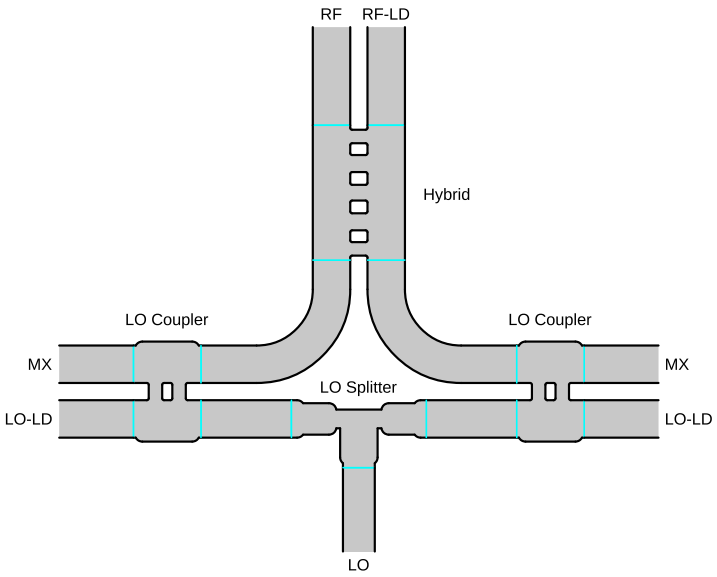

Figure 2. The central part of the waveguide structure. Port labels as follows. RF: input from feedhorn, RF-LD: RF load, LO: LO input, LO-LD: LO load, MX: mixer.

2.2 Design Drivers

Overall, we conclude that the key to achieve low noise temperature and high image rejection simultaneously is to make the waveguide structure as transparent as possible, and the loads as lossy. While this may seem obvious, we specifically decided to put the parameters that are traditionally optimized, namely the phase and amplitude balance of the hybrid, at lower priority. The main consideration is that especially the image rejection seems to be much more tolerant to phase and amplitude imbalance than to standing waves. Additionally, a significant contribution from the mixers to the amplitude imbalance can be expected, so perfecting the amplitude balance of the hybrid in itself clearly follows a law of diminishing returns.

After the discission above, the following drivers for the new waveguide structure were set:

- The waveguides shall be as low-loss as possible. This to be achieved both by material choice and waveguide dimensions.
- The waveguide loads shall be optimized to have (real-life) reflections of $-30\,\mathrm{dB}$ or lower.
- All waveguide components shall be optimized for low input and output reflections (possibly at the cost of amplitude/phase balance).

In the following sections, details about the implementation of these design rules will be given.

3. COMPONENT DESIGN

In this section we will present the geometrical design of the key components in the waveguide structure, together with results of numerical simulations. All simulations have been carried out with CST Microwave Studio. The geometrical details of the components can be found in appendix A.

3.1 Initial Design Choices

3.1.1 Waveguide dimensions

In view of the discussion of the resistive waveguide losses, the overall waveguide dimensions were chosen as large as reasonably possible: $400\times200\,\mu\mathrm{m}$. This gives a cutoff frequency of 375 GHz and, subsequently, a second cutoff of 750 GHz. Because of the closeness of the second cutoff to the top of the RF band (720 GHz), efforts were

Downloaded From: http://proceedings.spiedigitallibrary.org/ on 10/11/2016 Terms of Use: http://spiedigitallibrary.org/ss/termsofuse.aspx

taken to avoid any further widening in the structure. Except for one case (the LO coupler), this was achieved in all places.

Another reason to choose a waveguide width of 400 μm is the availability of left-over single-ended mixers from the ALMA Band 9 production.[8,9] These employed a reduced-height 400×100 μm waveguide, so no transitions in width (and hence, milling depth) have to be incorporated. The relatively high loss of a reduced-height waveguide was at the time no issue, because of the extremely short WG path involved. In the current structure the reduced height waveguides are tapered immediately to full-height as soon as they enter the hybrid block.

3.1.2 Minimal slot width

In order to facilitate machinability, a lower limit on any waveguide or slot width was set. Since most commonly available end mills on this scale have a maximum aspect ratio of 3:1, a minimum slot width of 72 μm (machinable with a 70×210 μm mill) was chosen. In one component, the LO coupler, a compromise with respect to the waveguide width had to be made in order to reach the desired performance while observing the minimum slot width.

3.1.3 Outer radii

Usually, all outer corners in the waveguide structures are left sharp. While this eases the simulations, it does not make for comfortable machining, as avoiding burrs on such corners can be quite challenging. Another reason to round off the corners slightly is the observation that, in simulations, often quite high current densities can develop there, with correspondingly, a potential for high losses. While some of these cases may be artefacts bacause of the finite mesh size in the simulation, it seems a good idea to avoid sharp corners as much as possible. In our design, a standard outer rasius of 10 μm was chosen. Obviously, the minimum inner radius is limited by the mill diameter of 70 μm, and set to 40 μm. As expected, the influences of the rounding on the component's properties can be compensated by slight modifications in the design dimensions.

3.2 Quadrature Hybrid

The quadrature hybrid is a standard five-branch coupler. Because of the closeness of the second cutoff, any widening of the waveguides beyond their standard height could lead to trapped modes.[10] For this reason, the coupler is of a simple straight design, as shown in Fig. 9. The amplitude and phase balance were first brought to their approximate goal values of 0 dB and 90°, respectively, by adjusting parameters s (branch length), with equal and equidistant branches (width g, spacing p). After this, the performance was optimized by slight variations in both position (P_1, P_2) and width (g_1 – g_3) of the individual slots. Figure 3a shows a representative set of

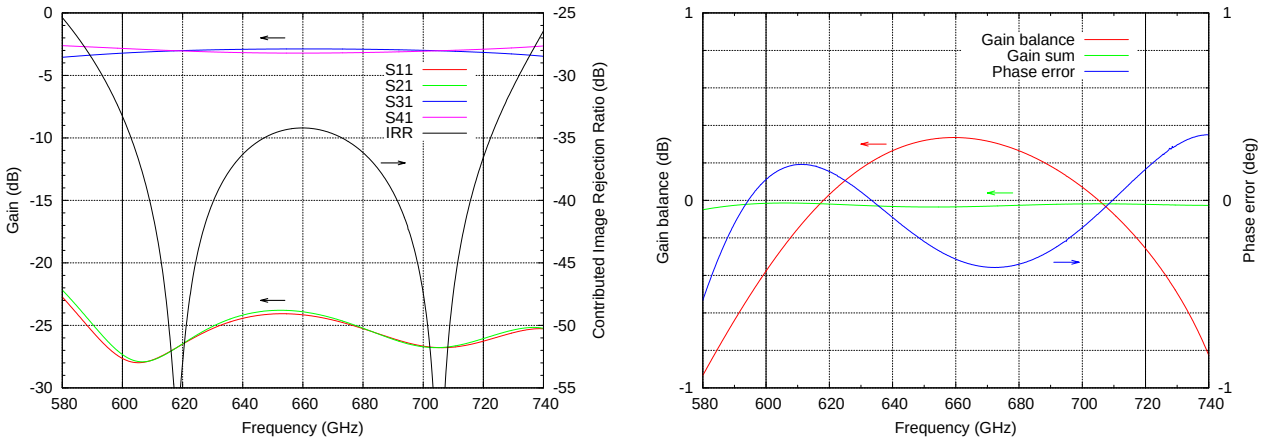

Figure 3. a (left): Representative set of S-parameters of the simulated hybrid and the hybrid's contribution to the image rejection ratio. Because of symmetry, each of the other S-parameters is identical to one of the four plotted ones. The vertical lines at 600 and 720 GHz indicate the band edges. b (right): The gain balance $|S_{31}|^2/|S_{41}|^2$, phase error $\arg(S_{31}) - \arg(S_{41}) - 90°$ and the total power throughput ("gain sum") $|S_{31}|^2 + |S_{41}|^2$.

Downloaded From: http://proceedings.spiedigitallibrary.org/ on 10/11/2016 Terms of Use: http://spiedigitallibrary.org/ss/termsofuse.aspx

simulated S-parameters for the resulting geometry. The resulting gain balance $|S_{31}|^2/|S_{41}|^2$ and phase error $\arg(S_{31}) - \arg(S_{41}) - 90°$, as well as the total power thoughput $|S_{31}|^2 + |S_{41}|^2$, are shown in Fig. 3b.

Within the chosen parameter space, it was found that there was a clear anti-correlation between input reflections and amplitude balance (and co-correlation with phase balance). In view of the preceding discussion of the standing wave issues, a high priority was placed on minimizing S_{11}, if necessary at the cost of amplitude balance. The resulting input reflection $|S_{11}|^2$ is lower than -24 dB over the entire band, while the amplitude imbalance is still within ± 0.4 dB. In Fig. 3a an additional curve is plotted of the hybrid's contribution to the image rejection ratio, *i.e.*, the expected IRR when all other involved components (mixers, IF hybrid) are perfect. The phase error is well within $\pm 0.5°$, which gives a negligible contribution to the IRR. As can be seen, the new hybrid design limits the IRR to about -34 dB. To illustrate the IRR-input reflection tradeoff: with slightly different set of parameters, an improvement of the theoretical IRR contribution by almost 5 dB in the band center can easily be obtained, but at the cost of worsening S_{11} by about the same amount. Considering the emphasis we put on reducing standing waves, we chose to use the former parameter set instead.

3.3 LO Coupler

The LO is coupled in with a conventional two-branch directional coupler, shown schematically in Fig. 10. Because of advances in LO technology, the availability of sufficient LO power is not such a limiting factor anymore, compared to when the original design was prepared. In order to minimize signal loss, we reduced the coupling factor from -9 dB to -13 dB, bringing the insertion loss down to 0.25 dB at most.

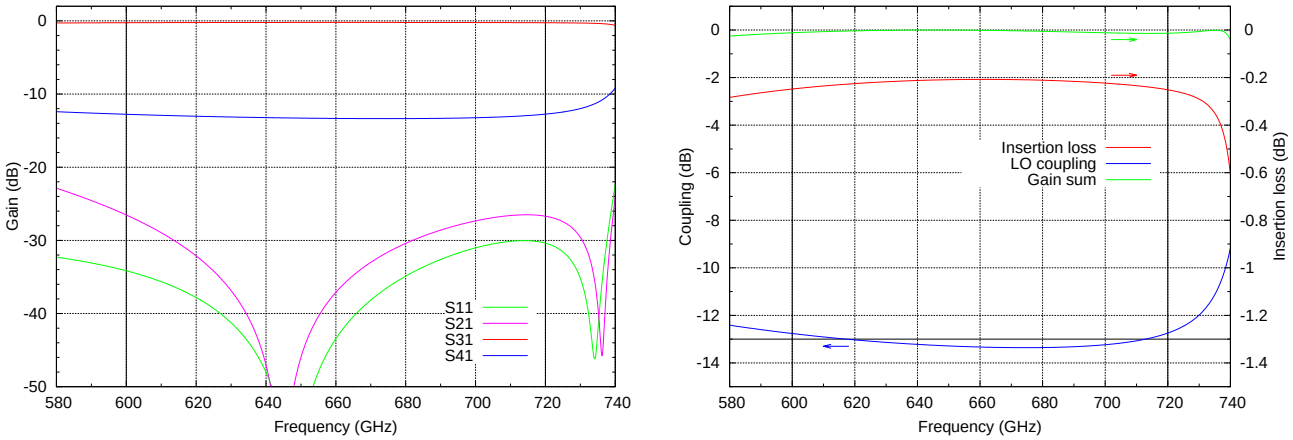

Figure 4. a (left): Representative set of S-parameters of the simulated LO coupler. b (right): Details of the LO coupling factor ($|S_{41}|^2$), insertion loss ($|S_{31}|^2$) and the total power throughput ("gain sum") $|S_{31}|^2 + |S_{41}|^2$.

Within the design constraints (mainly the minimum slot width and uniform channel depth), no solution with the desired low coupling factor was found. So, despite our intention not to broaden the waveguide anywhere (see section 3.1.1), we saw no other choice here. The widening helps to locally "dilute" the field sufficiently to reach a coupling factor of -13 dB without going under the minimum slot width.

Figure 4 shows the simulated S-parameters of the optimized model. Just as in the case of the hybrid, the design was optimized to get as low S_{11} as possible, mainly to minimize any standing wave between the coupler and the (relatively strong reflective) SIS mixer device. As can be seen, a modelled input reflection of -30 dB was obtained. Also important is the optimization the directivity (*i.e.*, $|S_{21}|^2/|S_{41}|^2$). Reason is that half of any LO power going this path will escape through the RF feedhorn, with many possibilities of causing phase and amplitide instabilities through low-level reflections off the IR filters, the window or the secondary reflector of the telescope.

3.4 LO Splitter

The LO is divided by an E-plane T-splitter with matching sections in all three legs, schematically shown in Fig. 11. The simulation results of the optimized geometry is in Fig. 5. The power division factor is, of course,

Downloaded From: http://proceedings.spiedigitallibrary.org/ on 10/11/2016 Terms of Use: http://spiedigitallibrary.org/ss/termsofuse.aspx

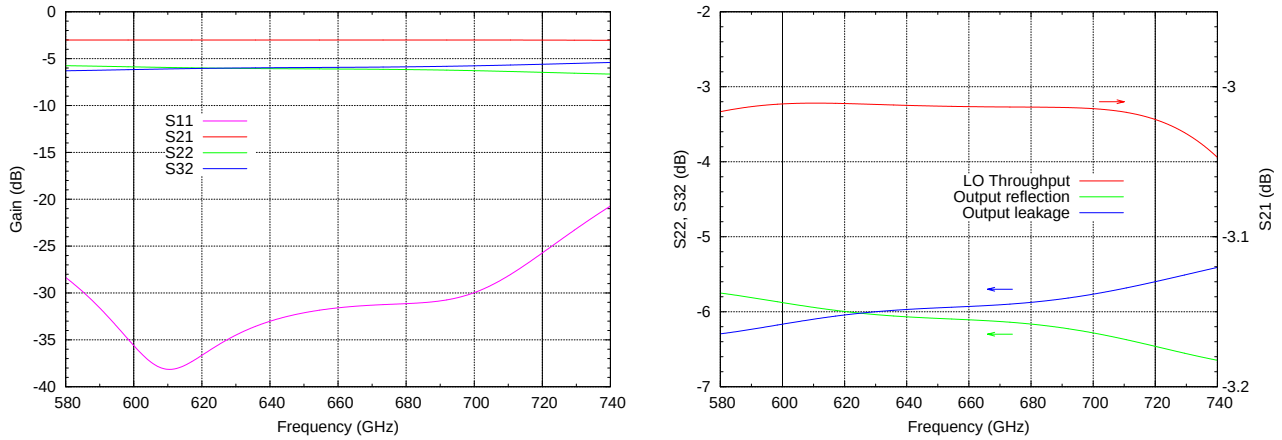

Figure 5. a (left): Representative set of S-parameters of the simulated LO splitter. b (right): Details of the LO throughput ($|S_{21}|^2$), the output reflection ($|S_{22}|^2$) and the output-to-output leakage ($|S_{32}|^2$).

purely defined by symmetry, which means the only things to optimize in an ideal model are the port reflections and isolation. Because the splitter is a non-dissipative three-port device (unlike, *e.g.*, a Wilkinson power divider), it has either highly reflective output ports (S_{22}, S_{33}) and/or low islolation between the latter (S_{23}, S_{32}). Because both inpact the standing wave issues in about the same way, they were chosen to be about equal (≈-6 dB). The input reflection of the LO input port (S_{11}) was minimized to avoid further problems with standing waves between the mixer block and the LO itself.

3.5 Loads

The main loads (hybrid termination and LO dump) are of the same concept as in the previous design: a waveguide running out at an oblique angle into a large cavity filled with absorbing material (Eccosorb MF112*). Despite its simplicity, these already worked surprisingly well there. The transition into the load-filled cavity shows a reflection of less than -30 dB in simulation. For this, a Lorentz oscillator model for the dispersion was used, as in the original monolithic design.[11] Despite efforts for cryogenic characterization of these types of materials (*e.g.*,[12]), their cryogenic high-frequency behavior remains an uncertainty. For instance, during preparation for the production of ALMA Band 5 receivers, it was found that a similar material (Eccosorb MF116), when used as an attenuator, may lose an order of magnitude in absorbtion between room temperature and 4 K. Since this contradicts earlier findings[13] to some degree, further investigation is in order.

Because of the uncertainties about the absorbing properties at 4 K and the high demands put on the loads in this mixer, additional attenuation was introduced in the form of a long stretch of waveguide coated with a high-loss material. Titanium was chosen for the coating for reasons of availability and ease of deposition. Its resistivity at 4 K depends, as most metals, heavily on its purity, but a value two orders of magnitude higher than that of copper can easily be expected, which translates to about an order of magnitude more loss per length unit than a pure copper waveguide.

The coated waveguides leading to the loads are about 20 mm long. Some experiments were performed on straight test waveguides coated in the same way, yielding an attenuation of at least 0.2 dB/mm. From this, we expect an additional round-trip attenuation (*i.e.*, improvement of S_{11} of the load) of about 8 dB.

3.6 Tapers

Because of the desired reuse of critical DSB Band 9 components (mainly the feedhorns and mixer backpieces), the waveguides have to be tapered back from 400×200 μm to the reduced-height dimensions of 400×100 μm used before. To minimize the added loss of the reduced-height waveguide path, the tapers are located as close to the interface plane as possible. Since each end of a taper presents a small source of reflections, the lengths of the tapers were chosen to be integral multiples of $\lambda/2$ to align the maximum of any passband ripple with the center of the band.

*Emerson & Cuming

Downloaded From: http://proceedings.spiedigitallibrary.org/ on 10/11/2016 Terms of Use: http://spiedigitallibrary.org/ss/termsofuse.aspx

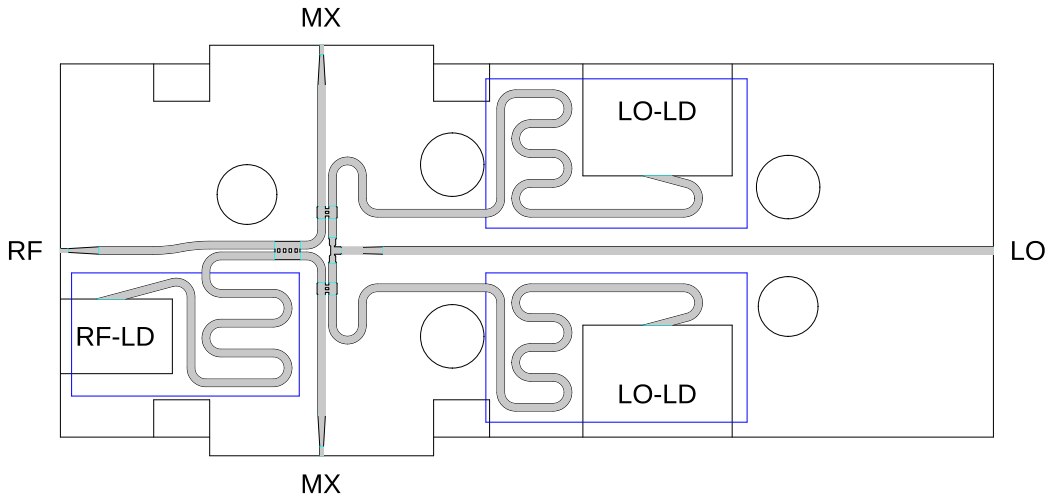

Figure 6. View on the split plane of the mixer block. RF: interface to RF feedhorn, LO: LO input, MX: interface to mixer back pieces, RF-LD: cavity for RF load material, LO-LD: cavities for LO load material. The blue rectangles indicate the areas to be coated with resistive layer.

3.7 Total Design

The envelope of the mixer block is identical to the one used previously.[4] The implementation of the complete waveguide structure is show in figure 6, with the areas to be sputtered with titanium indicated. To obtain sufficient attenuation, the coated waveguides leading to the loads have been folded several times.

4. RESULTS

A first prototype of the hybrid block was manufactured at the Universidad de Chile. It was equipped with exactly the same mixer devices, horns as other auxiliary components as used in the characterization of the previous design.[4]

The assembled mixer was tested in a modified copy of a standard ALMA band 9 receiver cartridge. The noise temperature was determined with a 300 K/77 K hot-cold Y-factor measurement, the image rejection ratio was measured according to the method described in.[14]

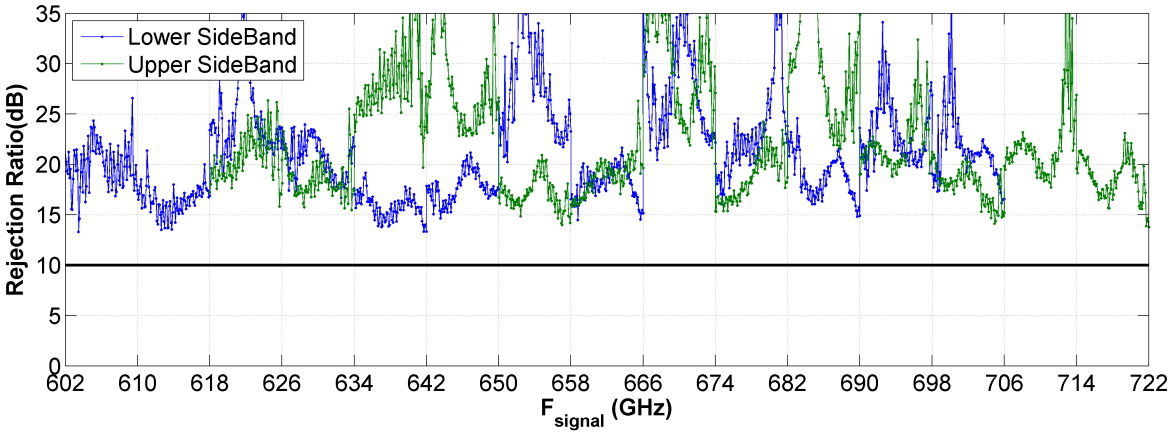

Figure 7. Preliminary measurement data of the image rejection ratio as function of RF input frequency. The ALMA specification (10 dB minimum IRR) is indicated with a horizontal line. Note that this data was obtained with an unifinished block.

Downloaded From: http://proceedings.spiedigitallibrary.org/ on 10/11/2016 Terms of Use: http://spiedigitallibrary.org/ss/termsofuse.aspx

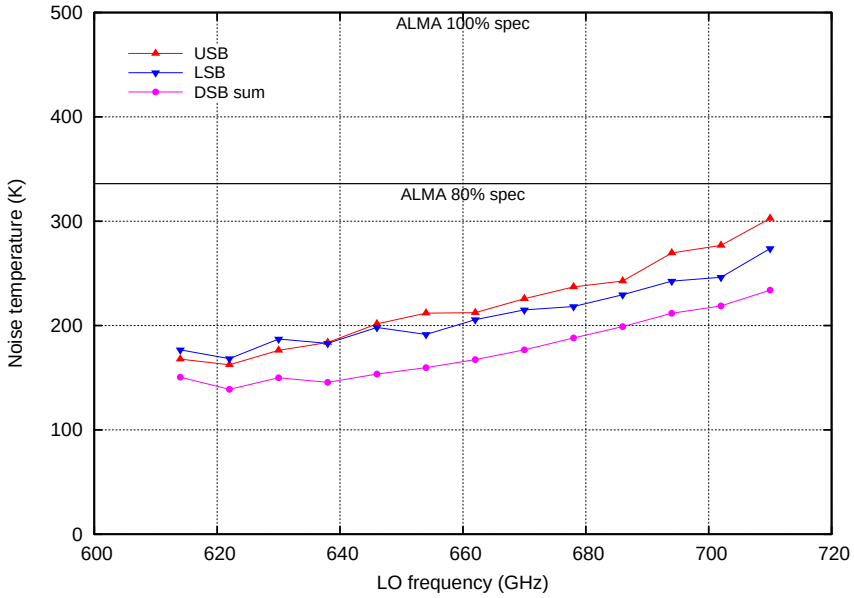

Figure 8. Preliminary noise data of both upper and lower sidebands as function of LO frequency. For reference, the sum of the DSB noise temperatures of the two individual SIS mixer devices is plotted as well. According to the ALMA Band 9 specifications, the SSB noise temperature should be below 336 K for at least 80% of the band, and below 500 K for the entire band.

The image rejection, shown in Fig. 7 is within the ALMA specification over the entiry band, with ample margin. Note that these are preliminary measurements. The hybrid block was not yet fully deburred and the titanium coating in the waveguide loads was not applied. We expect the image rejection still to improve considerably with a fully finished block.

The noise temperature for the two sidebands is shown in Fig. 8. Also here the ALMA specification is met with a wide margin. For comparison, in the latter figure also the sum of the noise temperatures of the individual mixer devices is plotted. Compared to this, the hybrid block incurs an excess noise temperature of about 30 K, corresponding to a waveguide loss of about 0.8 dB. Also here, we expect still some improvement when the block is finally fully deburred.

5. CONCLUSIONS

We completed a new design for a sideband-separating mixer assembly for 600–720 GHz that minimizes internal standing waves without introducing excess loss. Preliminary measurements with an unfinished block show that both the image rejection ratio and the noise temperature are already way within typical specifications for current observatories. The noise performance is now at the level that continuum observations, with the same total IF bandwidth, will not suffer significantly when compared to double-sideband instruments. Spectral observations, however, will benefit substantially.

ACKNOWLEDGMENTS

We would like to acknowledge José Pizarro (Universidad de Chile) for machining the hybrid block, and Mariëlle Bekema and Rob de Haan-Stijkel (Kapteyn Astronomical Institute) for their help integrating and measuring the mixer assembly. The envelope of the mixer block and the associated components were originally designed by Gerrit Gerlofsma. The waveguide design of the original hybrid block were due to Jacob Kooi. Also, we would like to recognize the efforts of the group led by T.M. Klapwijk producing the mixer devices during the ALMA Band 9 production. Finally, we thank Joost Adema and Albert Koops for their organizational and management support.

This work is part of the ALMA sub-mm instrumentation R&D project of NOVA, the Netherlands Research School for Astronomy.

Downloaded From: http://proceedings.spiedigitallibrary.org/ on 10/11/2016 Terms of Use: http://spiedigitallibrary.org/ss/termsofuse.aspx

APPENDIX A. DETAILS OF THE WAVEGUIDE STRUCTURES

Figures 9, 10 and 11 show the geometry of the waveguide components, with tables of the optimized dimensions. Parameter a is the waveguide width, *i.e.*, normal to the graphs. The encircled numbers identify the port numbers.

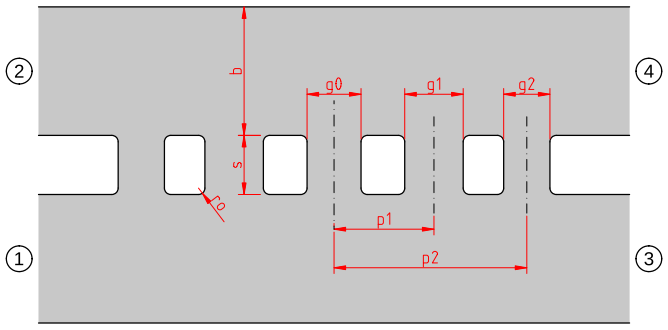

Dimension	μm
a	400
b	200
s	92
p_1	156
p_2	300
g_0	84
g_1	91
g_2	72
r_o	10

Figure 9. Dimensions of the quadrature hybrid

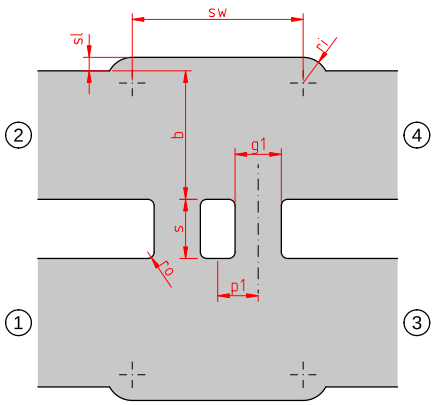

Dimension	μm
a	400
b	200
s	92
p_1	63
g_1	72
s_w	266
s_l	21
r_i	40
r_o	10

Figure 10. Dimensions of the LO coupler

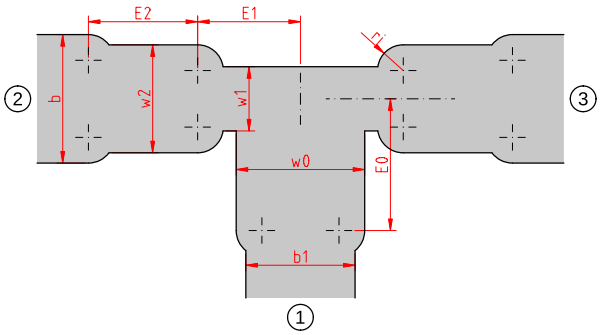

Dimension	μm
a	400
b	200
b_1	170
w_0	200
w_1	100
w_2	168
E_0	205
E_1	160
E_2	170
D	600
T	275
r_i	40

Figure 11. Dimensions of the LO splitter

Downloaded From: http://proceedings.spiedigitallibrary.org/ on 10/11/2016 Terms of Use: http://spiedigitallibrary.org/ss/termsofuse.aspx

REFERENCES

[1] Khudchenko, A., Hesper, R., Baryshev, A., Mena, F. P., Gerlofma, G., Zijlstra, T., Klapwijk, T. M., Kooi, J. W., and Spaans, M., "First results of the sideband-separating mixer for alma band 9 upgrade," in [*Twenty-Second International Symposium on Space Terahertz Technology, Charlottesville*], 143–149 (2011).

[2] Khudchenko, A., Hesper, R., Baryshev, A., Gerlofma, G., Barkhof, J., Adema, J., Mena, P., Klapwijk, T., and Spaans, M., "Sideband separating mixer for 600-720 ghz for alma band 9 upgrade," in [*Society of Photo-Optical Instrumentation Engineers (SPIE) Conference Series*], *Society of Photo-Optical Instrumentation Engineers (SPIE) Conference Series* **8452**, 14 (sep 2012).

[3] Mena, F., Kooi, J., Baryshev, A., Lodewijk, C., Zijlstra, T., Hesper, R., Gerlofsma, G., Klapwijk, T., and Wild, W., "Design and performance of a 600–720-ghz sideband-separating receiver using alo_x and aln sis junctions," *IEEE Transactions on Microwave Theory and Techniques* **59**, 166–177 (jan 2011).

[4] Hesper, R., Gerlofsma, G., Mena, F. P., Spaans, M. C., and Baryshev, A. M., "A sideband-separating mixer upgrade for alma band 9," in [*Twentieth International Symposium on Space Terahertz Technology, Charlottesville*], 257–260 (apr 2009).

[5] Baryshev, A. M., Hesper, R., Mena, F. P., Klapwijk, T. M., van Kempen, T. A., Hogerheijde, M. R., Jackson, B. D., Adema, J., Gerlofsma, G. J., Bekema, M. E., Barkhof, J., de Haan-Stijkel, L. H. R., van den Bemt, M., Koops, A., Keizer, K., Pieters, C., Koops van het Jagt, J., Schaeffer, H. H. A., Zijlstra, T., Kroug, M., Lodewijk, C. F. J., Wielinga, K., Boland, W., de Graauw, M. W. M., van Dishoeck, E. F., Jager, H., and Wild, W., "The alma band 9 receiver. design, construction, characterization, and first light," *A&A* **577**, A129 (may 2015).

[6] Pippard, A., "The surface impedance of superconductors and normal metals at high frequencies. ii. the anomalous skin effect in normal metals," *Proc. Roy. Soc.* **A191**, 385 (1947).

[7] Reuter, G. E. H. and Sondheimer, E. H., "The theory of the anomalous skin effect in metals," *Proc. Roy. Soc.* **A195**, 336 (1948).

[8] Zijlstra, T., Lodewijk, C. F. J., Vercruyssen, N., Tichelaar, F. D., Loudkov, D. N., and Klapwijk, T. M., "Epitaxial aluminum nitride tunnel barriers grown by nitridation with a plasma source," *Appl. Phys. Lett.* **91**, 233102–233103 (Dec. 2007).

[9] Lodewijk, C. F. J., Noroozian, O., Loudkov, D. N., Zijlstra, T., Baryshev, A. M., Mena, F. P., and Klapwijk, T. M., "Optimizing superconducting matching circuits for nb sis mixers operating around the gap frequency," *Applied Superconductivity, IEEE Transactions on* **17**, 375–378 (June 2007).

[10] Morgan, A. and Pan, S.-K., "Graphical prediction of trapped mode resonances in sub-mm and thz networks," in [*23rd International Symposium on Space Terahertz Technology, Charlottesville*], 39–42 (2012).

[11] Mena, F. P. and Baryshev, A. M., "Design and simulation of a waveguide load for alma band 9," in [*ALMA Memo Series*], Memo 513 (jan 2005).

[12] Ediss, G. A., Kerr, A. R., Moseley, H., and Steward, K. P., "Fts measurements of eccosorb mf112 at room temperature and 5 k from 300 ghz to 2.4 thz," in [*ALMA Memo Series*], Memo 273 (sep 1999).

[13] Kerr, A. R., Moseley, H., Wollack, E., Grammer, W., Reiland, G., Henry, R., and Steward, K. P., "Mf-112 and mf-116: Compact waveuide loads and fts measurements at room temperature and 5k," in [*ALMA Memo Series*], Memo 494 (may 2004).

[14] Kerr, A. R., Pan, S.-K., and Effland, J. E., "Sideband calibration of millimeter-wave receivers," in [*ALMA Memo Series*], Memo 357 (mar 2001).

Downloaded From: http://proceedings.spiedigitallibrary.org/ on 10/11/2016 Terms of Use: http://spiedigitallibrary.org/ss/termsofuse.aspx